AIP Journal of Applied Physics

Silver nano-entities through ultrafast double ablation in aqueous media for surface enhanced Raman scattering and photonics applications

G. Krishna Podagatlapalli, Syed Hamad, Surya P. Tewari, S. Sreedhar, Muvva D. Prasad et al.

Citation: J. Appl. Phys. **113**, 073106 (2013); doi: 10.1063/1.4792483
View online: http://dx.doi.org/10.1063/1.4792483
View Table of Contents: http://jap.aip.org/resource/1/JAPIAU/v113/i7
Published by the American Institute of Physics.

JOURNAL OF APPLIED PHYSICS **113**, 073106 (2013)

Silver nano-entities through ultrafast double ablation in aqueous media for surface enhanced Raman scattering and photonics applications

G. Krishna Podagatlapalli,[1] Syed Hamad,[2] Surya P. Tewari,[1,2] S. Sreedhar,[1] Muvva D. Prasad,[3] and S. Venugopal Rao[1,a)]

[1]*Advanced Center of Research in High Energy Materials (ACRHEM), University of Hyderabad, Prof. C.R. Rao Road, Hyderabad 500046, India*
[2]*School of Physics, University of Hyderabad, Prof. C.R. Rao Road, Hyderabad 500046, India*
[3]*Centre for Nanotechnology, University of Hyderabad, Prof. C.R. Rao Road, Hyderabad 500046, India*

(Received 16 November 2012; accepted 1 February 2013; published online 21 February 2013)

We have fabricated stable silver nanoparticles (NPs) and nanostructures (NSs) effectively through double ablation of bulk silver substrate immersed in double distilled water using ~2 ps laser pulses. The effects of multiple/double/single ablation on silver substrates via surface morphology studies along with average size distribution of Ag NPs were investigated. Prepared Ag NPs in solution exhibited yellow color with an absorption peak near 410 nm, assigned to localized surface Plasmon resonance of nano-sized silver. Depending on the ablation parameters average sizes observed were ~13 nm/~17 nm in multiple/double ablation case and ~7 nm in single ablation case. High resolution transmission electron microscope studies highlighted that most of the Ag NPs were spherical and polycrystalline in nature. Surface morphology of the substrates was characterized by field emission scanning electron microscope and atomic force microscope. A different scenario was observed in the double ablation case compared to single/multiple ablation case. Double ablation resulted in dome like NSs on the substrate with dimensions of few hundreds of nanometers while single ablation did not. Nonlinear optical (NLO) properties of Ag NPs were investigated using Z-scan technique with ~2 ps pulses and corresponding NLO coefficients were obtained. Surface enhanced Raman scattering (SERS) studies on multiple/double ablated Ag substrates with adsorbed Rhodamine 6G molecules were carried out using excitation wavelengths of 532 nm, 785 nm, and three orders of enhancement in Raman signal intensity was observed. Furthermore, influence of laser fluence on the fabrication of SERS active Ag substrates with double ablation was also investigated. In this case, Raman spectra of adsorbed Research Department eXplosive (RDX) molecules on ablated surfaces were recorded for 532 nm and 785 nm excitation. Enhancements up to 460 were observed from substrates fabricated at fluences of 12 J/cm^2, 16 J/cm^2 with excitation wavelengths of 532 nm and 785 nm, respectively.
[http://dx.doi.org/10.1063/1.4792483]

INTRODUCTION

Among diverse methods[1–4] investigated recently for fabrication of metallic nanoentities, ultrafast ablation in liquid media, based on the reaction dynamics of plasma and ambient species, is an uncomplicated technique to synthesize desired functional nanomaterials.[5–16] The technique is versatile and proficient for fabricating both metal nanoparticles and nanostructured substrates in a single experiment. Moreover, ablation in liquids afford extremely stable NPs with higher occupational safety since the fabricated NPs, generally, are in colloidal form.[17] The incident laser pulse initially interacts with the surface conduction electrons and later with the lattice through electron-phonon coupling. Comparison of pulse duration with the characteristic time scales of electron-phonon interaction indicates that there are two regimes of interaction. For longer pulses [typically >100 picosecond (ps)], thermal diffusivity determines the surface temperature which proceeds in equilibrium conditions. For sub-ps pulses (<1 ps), ablation proceeds in non-equilibrium conditions since the pulse duration is much shorter than the electron-phonon interaction time and electron heat conduction time implying that electrons cool without transferring the heat to lattice.[18] In this regime, threshold fluence is independent of the pulse duration. In the present study, ~2 ps pulses were utilized implying that the experiments were performed in the intermediate regime. It has also been established that maximum rate of metal ablation in liquids was achieved with 2 ps pulses.[19] Furthermore, ablation of metals in aqueous media generates nearly oxygen-free colloidal suspensions. The interaction of ultrashort laser pulses with metals in liquids and dynamics of the plume formation leading to generation of nanoparticles and surface modifications are fairly understood and documented.[20,21] During viscous interaction of liquid vapor with the molten layer, Rayleigh-Taylor or Kelvin-Helmholtz instabilities are encountered leading to the redistribution of metallic melt followed by formation of mushroom-like and dome-like structures on the surface.[22,23] Barcikowski *et al.* studied the dynamics of ablation of metals immersed in liquid media as the function of laser parameters and nature of

[a)]Author to whom correspondence should be addressed. Electronic addresses: svrsp@uohyd.ernet.in and soma_venu@yahoo.com.

surrounding liquid in detail.[24–27] These fabricated nano-entities exhibit novel electronic, optical, and other physical properties depending on their crystallinity, composition, shape, and size. Significantly, structured surfaces facilitate the momentum conservation of horizontal components of incident light wave vector and surface electromagnetic wave vector. Such a possibility is fundamental for surface Plasmon mediated Raman studies. Raman scattering, as such, is a weak process with extremely small cross sections (typically 10^{-31} to 10^{-26} cm^2), thus providing a poor signal to noise ratio (SNR). This situation generally fails to deliver essential, useful information of the important molecular fingerprints under investigation. To prevail over the ambiguity caused by poor scattering cross-sections many experimental techniques, for instance stimulated Raman scattering, coherent anti-stokes Raman scattering, surface enhanced Raman scattering (SERS) were investigated.[28–30] Among various techniques investigated, SERS is an efficient and simple method, has recently caused a great deal of excitement due to the fact that effective Raman cross-sections of molecules on a roughened silver surface (or a metal surface which can invoke SPR) can be enhanced up to 10^8 times compared to the same molecules dissolved in solution.[31–33] Several techniques have recently been employed to fabricate nanostructured surfaces.[34–37] The main effects that can be employed in SERS[38] are nano-sized colloidal suspensions and nanostructured substrates of plasmonic metals such as silver, gold, and copper. The electromagnetic model[39–44] elucidates the enhancements resulting from the amplification of incident and reradiated fields by the Plasmon resonances. SERS has great potential for applications in contrasting fields of biology, medicine, diagnostics, sensing, etc., and therefore, commercial fabrication of SERS active substrates remains an active challenge.[45] Despite numerous works on ablation in liquid media (pre-dominantly with nanosecond pulses), multiple/double ablation of metal targets (overwriting the metal substrate in liquid environment) has not yet been explored. In the present work, we extensively investigated the (a) nonlinear optical (NLO) properties of Ag colloids achieved through multiple/double ablation in double distilled water; (b) the effect of multiple/double ablation in defining the size, shape of the fabricated nano-entities on Ag surface and their SERS activity using R6G; (c) the influence of laser fluence on structures in the case of double ablation; and (d) Raman signal enhancements of 1,3,5-Trinitroperhydro-1,3,5-triazine [Research Department eXplosive (RDX)] molecules adsorbed on the nanostructured Ag substrates. The last part of the work is significant since identification of explosives[46–49] at very low concentrations in different environments is a predicament of critical interest for security and forensic diagnostics. Silver has been chosen because of (i) cost-effectiveness compared to gold, (ii) tendency towards oxidation is less compared to copper, and (iii) capacity to support strong Plasmon resonances. Amongst earlier reports Lee *et al.*[50] performed comprehensive study of SERS using the silver and gold nanoparticles as well as substrates fabricated in water via laser ablation with 6 ns laser pulses. However, they had studied the dynamics by focusing laser beam at a single point.

EXPERIMENTAL DETAILS

Ultrafast ablation was carried out using a chirped pulse amplified (CPA) Ti: Sapphire laser system (LEGEND, Coherent) delivering nearly transform limited laser pulses (~2 ps, 1 kHz repetition rate) at 800 nm. The amplifier was seeded with ~15 fs (55 nm FWHM) pulses from an oscillator (MICRA, Coherent, 1 W, 80 MHz, 800 nm central wavelength). Ag substrate submerged in double distilled water (2–3 mm above the Ag sample) in a Pyrex cell was placed on a motorized X-Y stage. Plane polarized (s-polarization) laser pulses were allowed to focus vertically onto the Ag substrate through a plano-convex lens of focal length 25 cm. The position of the focus was approximated to lie at the point where plasma was generated. X-Y translation stages, interfaced to Newport ESP 300 motion controller, were utilized to draw periodic structures on the Ag substrate with separations of 5 μm, 25 μm, 50 μm, and 75 μm. Typical energy used was ~150 μJ per pulse. For example, in the case of 5 μm, a structure was initially drawn on the Ag substrate through the movement of X-stage followed by vertical movement of 5 μm (using Y stage) and second structure was drawn on the substrate through the movement of X-stage in opposite direction. Thus, ablation was carried out for 25 μm, 50 μm, and 75 μm separations. Details of the experimental setup are provided in our earlier works.[11] The schematic of multiple/double/single ablation carried out on the Ag substrate is explained in Figures 1(a) and 1(b). The scanning speeds of the X-Y stages were 0.4 mm/s and 0.5 mm/s. The prepared Ag colloids are designated as NP-1, NP-2, NP-3, and NP-4, and the corresponding substrates as SS-1, SS-2, SS-3, and SS-4 for separations of 5 μm, 25 μm, 50 μm, and 75 μm, respectively. As per the mechanism shown in Figure 1, SS-1 was influenced by multiple ablations, whereas SS-2 was influenced by double ablation, since the estimated beam waist on the Ag substrate was >20 μm. Consequently, complete overwriting (ablation of pre-ablated portion) was carried out for SS-1 and partial overwriting for SS-2. Apart from these, SS-3 and SS-4 were obtained through single

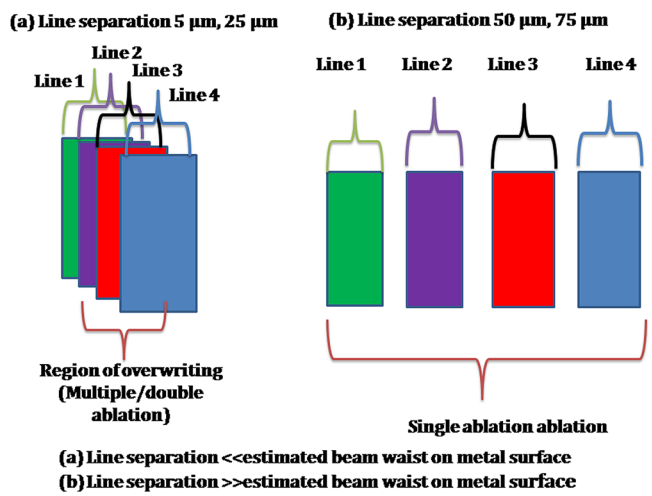

FIG. 1. (a) Mechanism of multiple/double ablation as a result of over writing for substrates SS-1 and SS-2. The separation between the scans was much less than the beam waist, (b) For SS-3, SS-4 ablation was carried out with separation more than beam waist.

ablation. Furthermore, Ag substrates (for a fixed scan separation of 20 μm) were also fabricated at different fluences of 4 J/cm^2, 8 J/cm^2, 12 J/cm^2, 16 J/cm^2, and 20 J/cm^2. To achieve superior fabrication rate of nanoparticles laser beam should be focused exactly on the surface of substrate. The uncertainty in adjusting focus exactly on the metal substrate because of the displacement caused by refractive index of the surrounding liquid and other nonlinear optical effects was taken care by observing the plasma.[51] The theoretical beam waist (ω_0) estimated at the focus (in air) was $\sim$10 μm while the dimensions of fabricated structures were measured to be $\sim$20 μm in the single ablation case. Subsequent to the completion of scan, Ag substrates were removed from the liquid and preserved after proper cleaning. Colloidal suspensions were preserved in air tightened glass vials.

The absorption spectra of obtained colloidal solutions and laser exposed substrates were recorded immediately using a UV-Vis spectrometer (Jasco-V-670 spectrometer) equipped with integrating sphere in the spectral range of 250–2500 nm. The EDX spectra and HR-TEM images of the NP-1, NP-2, NP-3, and NP-4 were recorded to identify the metallic finger prints and NP size distribution along with their crystallographic information. Morphology of the laser exposed portions of SS-1, SS-2, SS-3, and SS-4 were characterized by FESEM (Ultra 55 from Carl ZEISS) and an AFM. The NLO properties of NPs colloidal solutions were investigated using open and closed aperture Z-scan method[52] with 1 kHz, 800 nm laser pulses ($\sim$2 mJ, $\sim$2 ps duration). Complete details of the setup and procedures for evaluating the NLO coefficients are reported in our earlier works.[53–58] The performance of Ag substrates was evaluated by means of enhancement in Raman signal from adsorbed R6G molecules (typically μM concentrations). The substrates SS-1, SS-2 were immersed in R6G solutions for 2–3 hours to ensure strong adsorption of the molecules on patterned surface. Raman signals from R6G/RDX adsorbed substrates were collected using micro-Raman and bulk Raman spectrometers, which used continuous wave (cw) Nd:YAG laser at 532 nm and cw Ar^+ laser at 785 nm, respectively. Raman spectra of analytes from the structured surfaces were compared with the Raman spectra of analytes recorded from the plain surface. The input power of laser was $\sim$5 mW. The acquisition time for each measurement was 5 s, and all spectra were calibrated with respect to a silicon wafer at 520 cm^{-1}. In the Micro Raman spectrometer (excitation wavelength used was 532 nm), laser beam was focused on to the substrate using an objective lens (100X) and beam waist at the focus was near to 600 nm. In bulk Raman spectrometer (excitation wavelength-785 nm), laser beam (diameter 1 mm) was directed towards the sample without any focusing lenses and Raman signals were in the back scattering geometry.

RESULTS AND DISCUSSION

Characterization of Ag suspensions

Suspensions of Ag NPs were characterized by TEM (SEI cecnai G2 S-Twin 200 kV instrument) providing an estimate of size distribution and morphologies of the nanoparticles. Ag

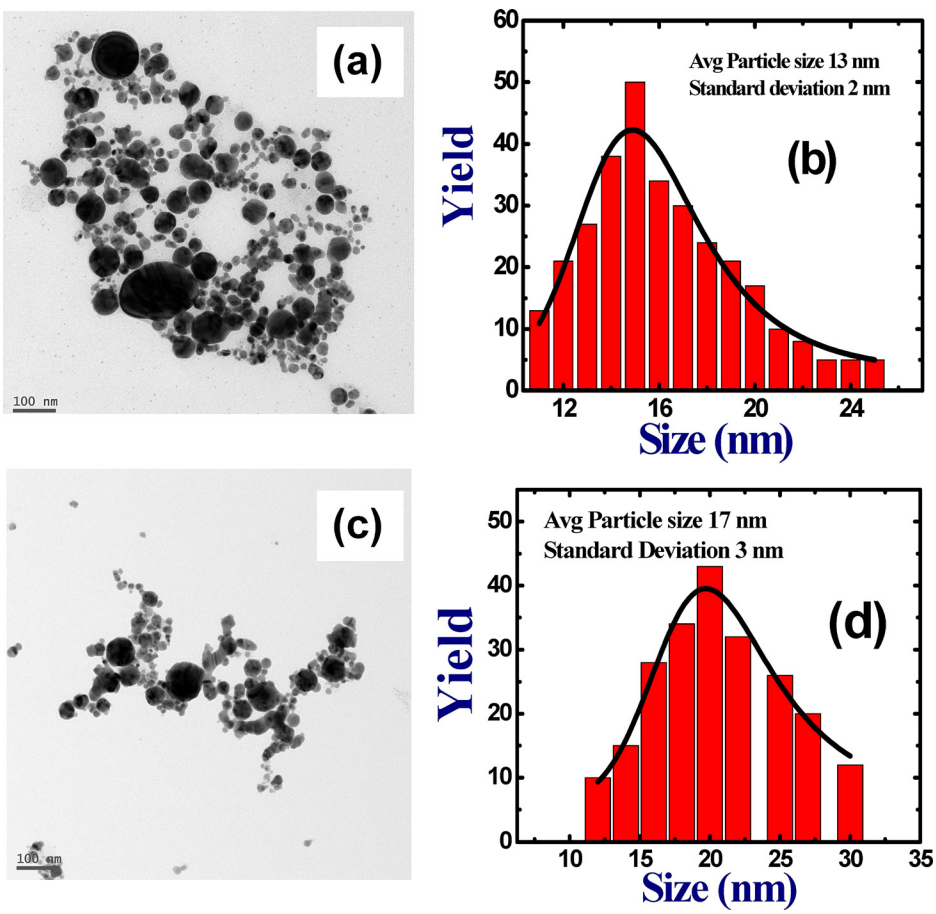

FIG. 2. Depiction of nanoparticles fabricated by pulsed ($\sim$2 ps, 800 nm) laser ablation of Ag metal immersed in double distilled water (a) TEM image of well dispersed Ag nanospheres formed in colloidal water (NP-1), (b) Size distribution histogram of Ag nanoparticles in NP-1 showing an average size near of 13 nm, (c) TEM image of Ag nanospheres in NP-2, (d) Size distribution histogram Ag nanoparticles in NP-2 exhibited an average size of 17 nm. The scale bar in (a) and (c) is 100 nm.

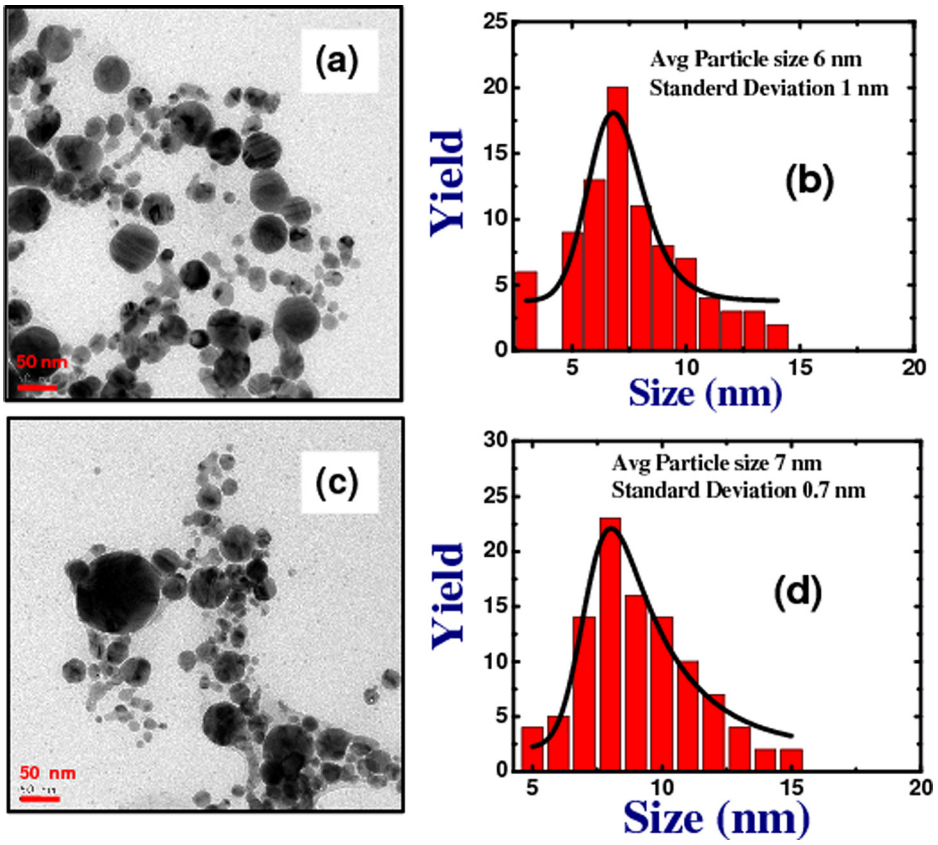

FIG. 3. Depiction of nanoparticles fabricated by pulsed (∼2 ps, 800 nm) laser ablation of Ag metal immersed in double distilled water. (a) TEM image of well dispersed Ag nanospheres formed in colloidal water (NP-3), (b) size distribution histogram of Ag nanoparticles in NP-3 depicting an average size of 6 nm, (c) TEM image of Ag nanospheres in NP-4, (d) size distribution histogram Ag nanoparticles in NP-4 demonstrated an average size of 7 nm. The scale bar in (a) and (c) is 50 nm.

colloids were centrifuged on carbon coated copper grids and analyzed using TEM operated at 200 keV. Figure 2 depicts the TEM pictures and size distributions for NP-1 and NP-2 while the corresponding data for NP-3 and NP-4 are illustrated in Figure 3. Figure 2(a) shows well dispersed spherical Ag nanoparticles (NP-1) and 2(b) shows the range (11 nm–25 nm) of size distribution with an average size of ∼13 nm. Figures 2(c) and 2(d) depict the TEM image of Ag nanoparticles sized 12–30 nm [NP-2 average size was ∼17 nm] and their size distribution, respectively. Similarly, Figures 3(a)–3(d) illustrates the TEM images along with the size distribution of NP-3 and NP-4. Average nanoparticle sizes in NP-3

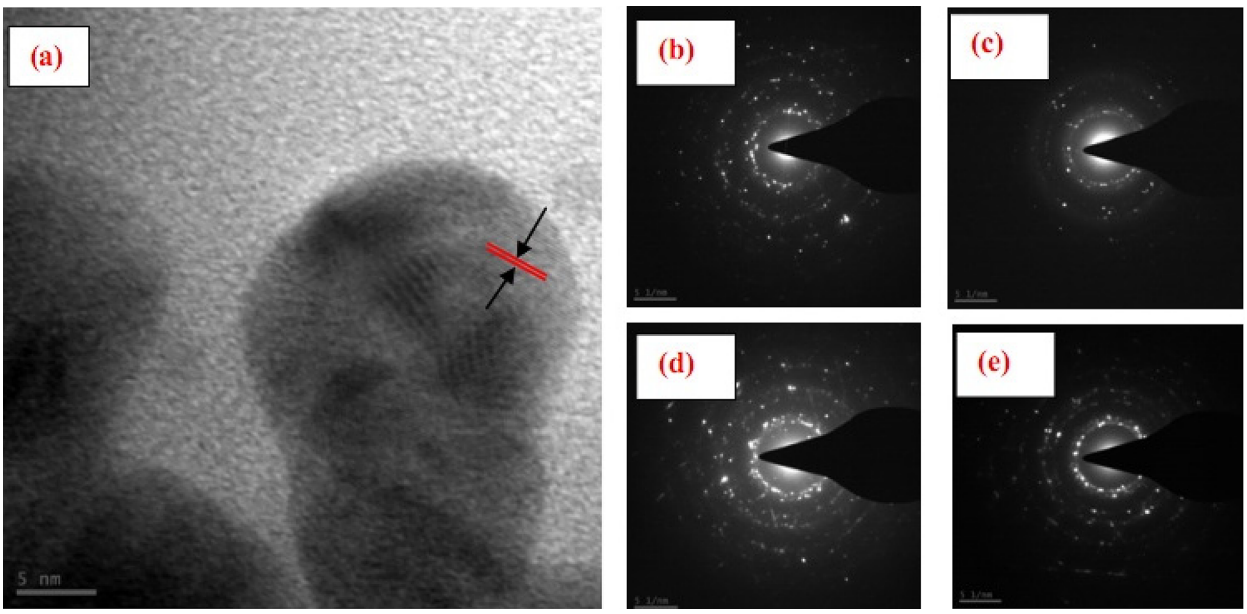

FIG. 4. (a) HRTEM image of the Ag nanoparticles formed shows the clear view of lattice planes observed at a characteristic separation 2.2 Å (diameter of the ring very next to the central maxima in the electron diffraction pattern) corresponding to the plane of Ag crystal (111). Right (b-e) – depictions of selective area electron beam diffraction patterns from the fabricated Ag nanoparticles in NP-1, NP-2, NP-3, and NP-4, respectively, confirming the polycrystalline nature of Ag nanocrystals. The scale bar in (a) is 5 nm.

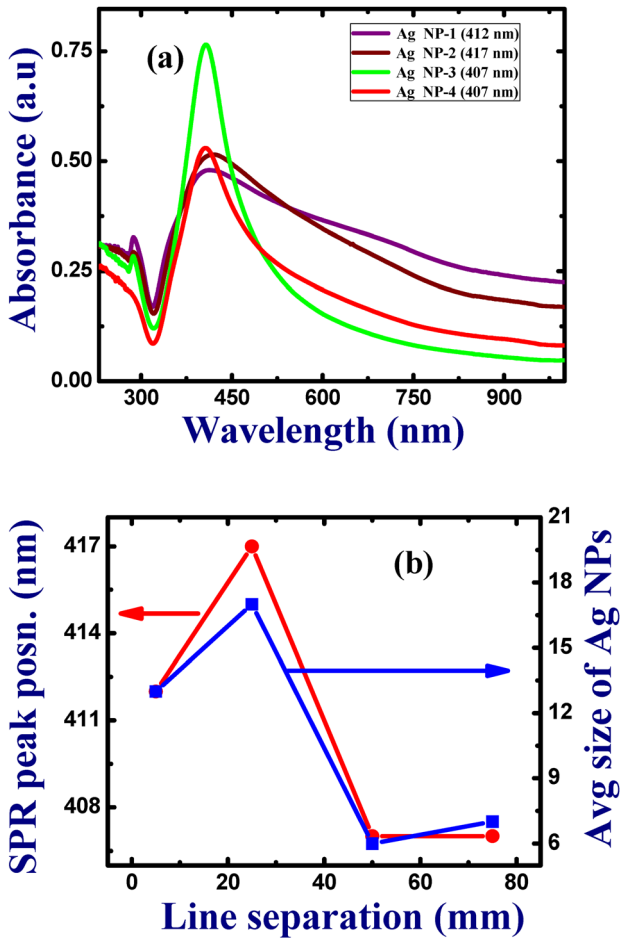

FIG. 5. (a) UV-Vis extinction spectra of Ag nanoparticles prepared in water (I) NP-1with SPR peak at 412 nm, (II) NP-2 with SPR peak at 417 nm, (III) NP-3 with SPR peak at 407 nm, (IV) NP-4 with SPR peak at 407 nm, (b) red curve depicts the variation of SPR peak with respect to line separation, blue curve depicts the average Ag particle size versus line separation.

(range of 3–14 nm) and NP-4 (range of 5–15 nm) were ~6 nm, ~7 nm, respectively. From the size distributions and average sizes, it was confirmed that the ablation was slightly different for nanoparticles in NP-1, NP-2 compared to nanoparticles NP-3, NP-4 even though all the exposure parameters were same except the overwriting part in the later cases. Figure 4(a) shows the HRTEM image of a single Ag nanoparticle exhibiting parallel Ag lattice planes having a separation 2.2 Å (indicated with a red mark in the figure) corresponding to (111) lattice planes of silver. Selective area electron diffraction patterns, shown in Figures 4(b)–4(e), revealed the polycrystalline nature of the Ag nanospheres for all the four cases. The variation in the average sizes of Ag nanoparticles was again established through the observed SPR peak position in the UV-visible absorption data. The fabricated particles were dispersed in water leading to coloration (light to golden yellow) of the solvent. The time of laser exposure in all four cases was identical. The recorded UV-visible absorption spectra of NP-1, NP-2, NP-3, and NP-4 exhibited LSPR peaks in the neighborhood of 412 nm, 417 nm, 407 nm, 407 nm, respectively, as illustrated in Figure 5(a). Figure 5(b) shows the variations of SPR peak position and average Ag nanoparticle size with respect to the scan separation. The position of SPR peak depends on the size distribution of Ag nanoparticles. Due to incubation[59,60] effects, we expect different sized NPs to be formed for NP-1 and NP-2.

Multiple/double and single ablation were carried by controlling the translational stages which were operated at scan speeds of 0.4 mm/s (X-stage) and 0.5 mm/s (Y-stage). The pulse repetition rate was 1 kHz implying a delay of 1 ms between two consecutive pulses. Estimated beam waist on the metal surface in water was 20 μm (ω_0). The estimation was based on the observed line structure width ($2\omega_0$ was 40 μm) from SEM images in single ablation case. Between two pulses, X-stage traversed a distance of 0.4 μm during ablation. Liang *et al.*[59] and Nielsen *et al.*[60] discussed the effect of incubation on higher yield NPs, the arguments of which can be extended to the higher yield of NP-1 and NP-2 observed in our case. Effective number of pulses per shot is calculated from ω(z)/d, where ω(z) is the beam waist on the surface of Ag, d is the pulse spacing. In our case of single ablation, the effective number of pulses per spot was 50 since ω(z) was ~20 μm and "d" was 0.4 μm. In the case of double ablation, the effective number of pulses per spot was 100. The case of multiple ablations is slightly complicated since the structure width created was 40 μm [using a ω_0 of 20 μm], and the stage was translated by ~5 μm for each scan. Therefore, we expect a gradient in the number of incident pulses (perpendicular to the scan direction) and consequently the ablation to be inhomogeneous. However, an average of 250 pulses per spot is estimated for the regions of observation since the SEM images and SERS spectra were collected from the central portion of ablated structure. For ablation in the case of NP-1 and NP-2, incubation effects are expected to play a major role. In these cases, increment in the effective number of pulses per spot decreases the ablation threshold dramatically[59,60] leading to the formation of metallic melt in large volume which acts as the reservoir resulting in higher yields of Ag nanoparticles. Incubation effects were observed in fs ablation of dielectrics such as fused silica.[59] Nielsen *et al.*[60] studied the fs ablation of metals (Cu, Ag, W) and observed the strong dependence of incubation effects on ablation threshold. In their case, the ablation threshold reduced (by almost 6 times) with increasing number of incident pulses (300). Similar incubation effects were observed for fs ablation experiments on stainless steel, Cu, Nb, and Ti.[61] However, these effects were observed in experiments performed with fs pulses and in air. There are not many reports available till date to understand the mechanisms of incubation effects during ablation in liquids. In our case, we performed experiments with ps pulses and in liquids. We do expect a similar incubation effect (though to a different degree yet to be ascertained through separate experiments) resulting in (a) reduction of ablation threshold (availability of more energy per ablation) and (b) creation of a structured target (through initial ablation) for subsequent ablations.

In the case NP-1, we anticipate a complete overlap of the ablation regions (separation of 5 μm), whereas in the case of NP-2, only a partial overlap is expected (separation of 25 μm). Ablation conditions for SS-1, SS-2 were different from those used for SS-3, SS-4 cases, and therefore, the fabricated sizes of Ag NPs will be different. According to two

temperature model,[62] there are two regimes wherein either skin depth or heat diffusion processes are dominant. These two regimes occur at different laser fluences on the target surface. Formation of different sized nanostructures is determined critically by the surface roughness. Furusawa *et al.*[63] investigated the ablation dynamics of plasmonic metals as a function of fluence and roughness with laser pulses of duration in the range of 120–800 fs. In case of ablation of rough metal surfaces, melting occurs in areas with weak thermal bonding to the substrate, e.g., in the vicinity of micro-relief, edges of scratches, etc., and consequently they observed dome like nanostructures on the substrate.[64] A comprehensive study of the ablation of metals in liquid medium was performed by Stratakis *et al.*[65] and demonstrated diverse surface dynamics under different experimental conditions. In our case, we expect that the ablation of pre-ablated substrate occurs multiple times on SS-1 since the separation between the two line structures (5 μm) was less than the estimated spot size on substrate ($2\omega_0 = 40\,\mu$m). Ablation for the first time creates initial roughness (micro-protrusions) on the substrate. When the ablation is carried out for the second time (on the first ablated portion), roughness offered will not be uniform leading to inhomogeneous melting of tips and micro-protrusions. An ideally polished surface will not melt below threshold laser intensity, whereas a roughened surface would offer loosely bound micro-protrusions to the laser beam which decrease the ablation threshold resulting in higher yield of NPs.[60] Because of this we could also observe larger range of NPs distribution in the case of double ablation which accounts for the broad Plasmon band in UV-Vis absorption spectra of NP-1 and NP-2. Nielsen *et al.*[60] demonstrated that the roughness provided by ablation for overwriting caused laser induced surface Plasmons and surface scattered waves which led to the coupling of laser energy to the modified surface in the next step of overwriting. This sort of energy coupling could be higher in the case of NP-1, NP-2 compared to NP-3, NP-4 since the former was affected by overwriting where as the latter experienced only single ablation.

In the UV-Vis absorption spectrum of NP-1 and NP-2, main resonance peak was observed in the neighborhood of 400 nm which is their characteristic surface Plasmon resonance which can be attributed to the intraband transitions from ground states of conduction band to excited states of conduction band. In the case of NP-3 and NP-4, size distribution (3–15 nm) of fabricated Ag NPs was less (compared to NP-1 and NP-2) which led to the observation of a sharp SPR band rather than a broad band. In NP-1 size distribution of Ag, NPs was ~11–25 nm and it was ~12–30 nm in NP-2. Garcia *et al.*[66] have demonstrated that the size dispersion of Plasmonic nanoparticles induces a broadening of the absorption peak. Some of the Ag NPs with large average size were not considered (very few in number) while constructing the histogram. Probably the SPR of these larger particles or oxidized Ag NPs resulted in a weak absorption peak near 650 nm. Further, Schinca *et al.*[67] investigated the effect of core and shell sizing (silver and silver oxide) on the red shift of absorption peak. Further investigations are pending to accurately point out the mechanism responsible for observing this weak peak. Since nanoparticles in NP-1 and NP-2 are close enough they experience a net electric field at the nanoparticles site due to (a) that of the incident light and (b) the field created by the rest of NPs. Therefore, resonance conditions will be modified resulting in a red shift of the SPR band[66] towards 412 nm. In a similar manner, a red shift of SPR peak to 417 nm was observed in NP-2. Observed red

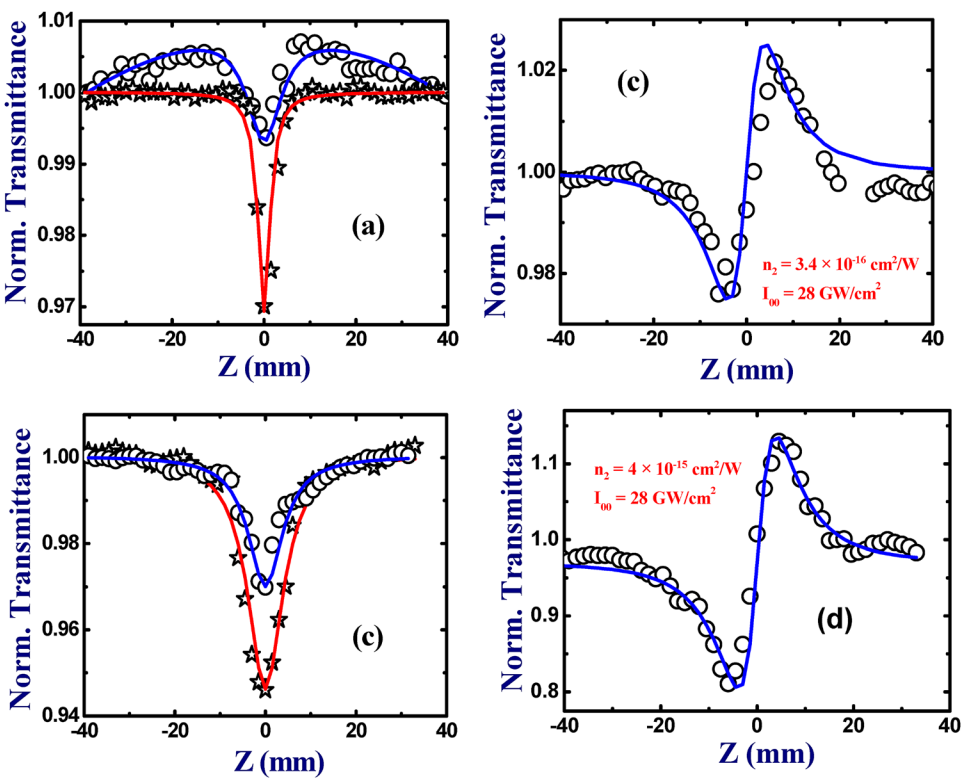

FIG. 6. Open aperture Z-scan curves obtained for (a) Ag colloids NP-1 with varying input intensities $I_{00} = 83$ GW/cm^2 (open circles), $I_{00} = 138$ GW/cm^2 (stars). Blue, red colors represent low intensity, high intensities, respectively, (b) closed aperture Z-scan curves obtained for Ag colloids NP-1 at peak intensity 28 GW/cm^2, (c) open aperture Z-scan curves obtained for Ag colloids NP-2 with varying input intensities $I_{00} = 83$ GW/cm^2 (open circles), $I_{00} = 138$ GW/cm^2 (stars), and (d) closed aperture Z-scan curves obtained for Ag colloids NP-2 at peak intensity 28 GW/cm^2. Solid lines are the theoretical fits.

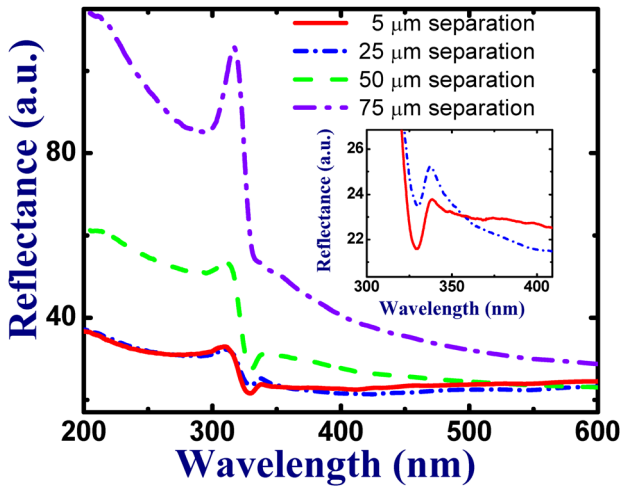

FIG. 7. UV-Vis reflectance spectra of the Ag substrates SS-1 (red, solid curve), SS-2 (blue, short dash-dot curve), SS-3 (green, dashed curve), and SS-4 (violet, dash-dot curve). A small hump (inset) near 340 nm confirmed the formation of nanostructures on SS-1 and SS-2. For the other two cases, no nanostructures were found.

shift of the SPR peak position of NP-1, NP-2 can also be explained from the effective medium theory (EMT) also wherein the modification of dielectric function of the medium as the function of separations of NPs. EMT explains that shorter the distance (since the yield is high), lower the resonance frequency (higher wavelengths).[68] SS-3 and SS-4 experienced single ablation since the separation between the line structures was greater than the estimated beam waist on the metal surface resulted in fine (~7 nm) nanoparticle fabrication. NP-3 and NP-4 exhibited SPR peaks near 407 nm. UV-Visible absorption spectra recorded for the colloids after 3–4 weeks depicted SPR peaks without significant change in their position suggesting the stability of these Ag colloids.

It was recently demonstrated that NLO characterization of freshly prepared Ag colloids presents large nonlinearities and are poorly reproducible.[69] Therefore, the NLO study (of NP-1 and NP-2) was performed on the colloids 1 day after fabrication. Figures 6(a) and 6(b) depict the open and closed aperture data of Ag colloids [Ag NP-1, Ag NP-2]. Open aperture Z-scan was carried out at peak intensities of 83 GW/cm^2 and 138 GW/cm^2, while the closed aperture data were recorded at 28 GW/cm^2. Open aperture data of NP-1 [linear transmittance (LT) ~90%] presented in Figure 6(a) demonstrated switching behavior [from saturable absorption (SA) to reverse saturable absorption (RSA)] with a saturation intensity of 6.5×10^7 W/cm^2 at lower peak intensity (83 GW/cm^2, $\beta = 2 \times 10^{-12}$ cm/W). RSA with a strong two-photon absorption coefficient ($\beta = 4.5 \times 10^{-12}$ cm/W) was observed at higher peak intensities (138 GW/cm^2). The experimental data

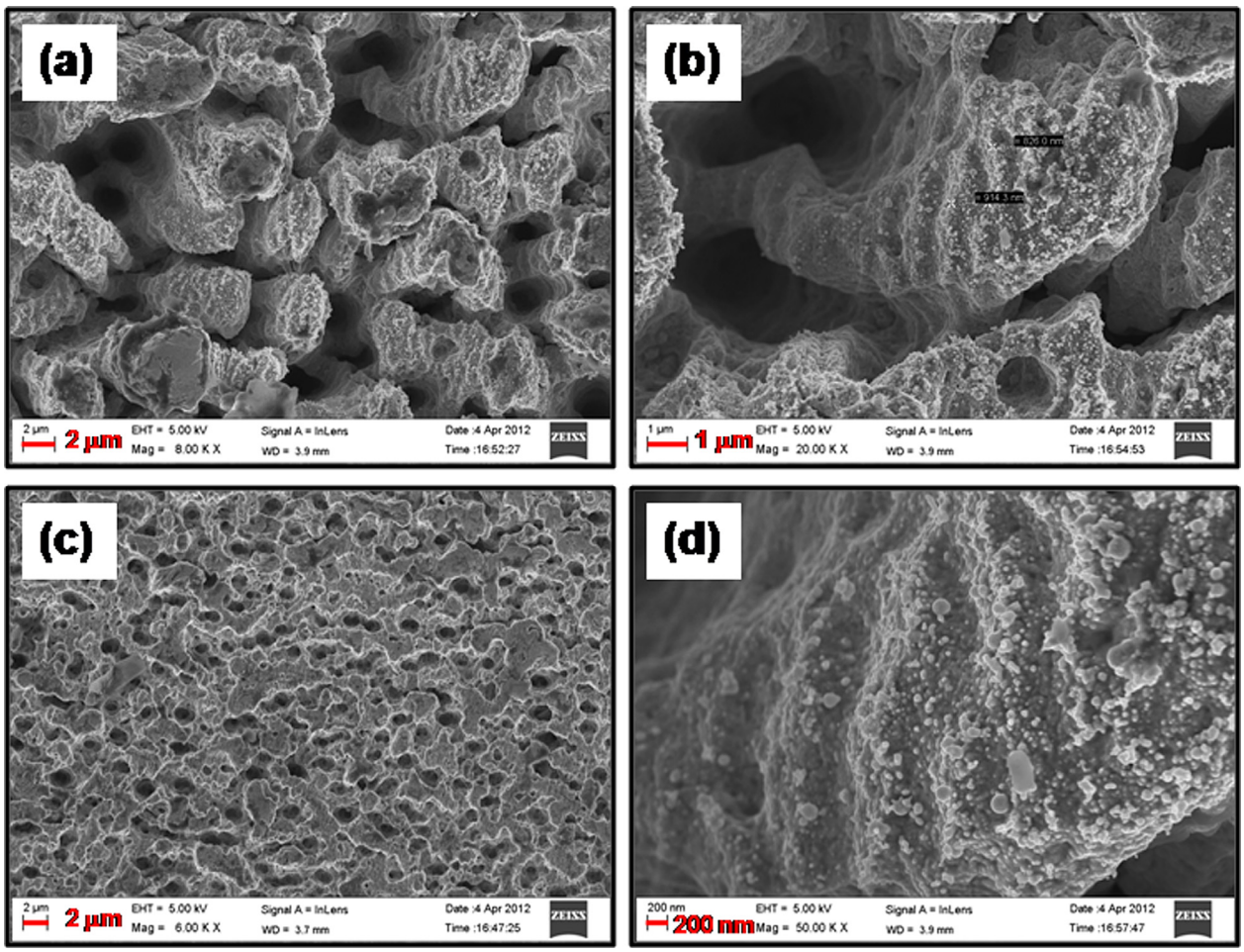

FIG. 8. FESEM images of the laser exposed portions in Ag substrate in water (a, b) dome like structures formed on the substrate SS-1 because of the over wring and its closer view, (c, d) surface morphology of SS-2 shows the dome like structures. Closer view images show the fabricated Ag NPs grains on the substrate. The scale bar in (a), (b), and (c) is 2 μm while in (d) it is 200 nm.

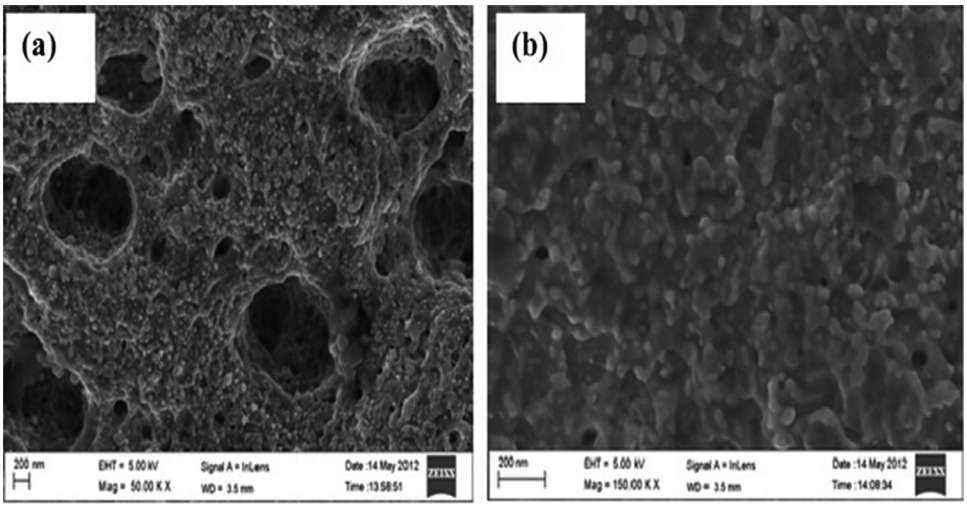

FIG. 9. FESEM images of the laser exposed portions of Ag substrate in water for (a) SS-3, fabricated at a line sparation of 50 μm,(b) SS-4, fabricated at a line sparation of 75 μm. The scale bar in (a) and (b) is 200 nm.

were fitted using standard equations.[53,55] The closed aperture data were fitted[70,71] to extract the nonlinear refractive index (n_2). NP-1 exhibited positive nonlinearity, as shown in Figure 6(b), and the measured n_2 was 3.4×10^{-16} cm^2/W. Figure 6(c) shows the open aperture data of NP-2 [linear transmittance (LT) ~92%] indicating pure RSA for both lower ($\beta = 6.2 \times 10^{-12}$ cm/W) and higher ($\beta = 1.78 \times 10^{-11}$ cm/W) peak intensities. The closed aperture data for NP-2 are shown in Figure 6(d) and n_2 retrieved from the fits to experimental data was 4×10^{-15} cm^2/W. Closed and open aperture data of the solvent (water) were also recorded. The n_2 value of the solvent was higher than the n_2 of NP-2 indicating that the sign of n_2 of NP-2 was negative. The measured $\chi^{(3)}$ (third order NLO susceptibility) values for NP-1 and NP-2 were 2.29×10^{-14} e.s.u, 2.69×10^{-13} e.s.u, respectively. The values of nonlinear coefficients presented here with an error bar of $\pm 10\%$ due to errors in the fits, estimation of spot size, etc. Observed switching (from SA to RSA) and pure RSA of the Ag NPs can be attributed to the intraband transitions. Following excitation with 800 nm photon (~1.55 eV), intraband electronic excitation within the conduction band might occur at lower intensities leading to ground state Plasmon band bleach, and therefore, SA was observed. Further pumping (higher peak intensities) could result in RSA, since the carriers can be excited from the ground state to high lying excited states of conduction band through two-photon (1 + 1) processes.[53] Furthermore, the energy of the photon at 800 nm is much less than the energy required causing interband (4d-5s for Ag) transitions in Ag (~4 eV) which explains the observed nonlinear phenomenon was not because of inter band transition but only intraband transitions. Gurudas *et al.*[72] observed SA (lower peak intensities) and RSA (higher peak intensities) in Ag nanorods with ~25 ps pulses at 532 nm. In their case, the excitation was close to the Plasmon resonance, whereas we are away from the absorption peak resulting in a switching behavior.

Characterizations of the Ag substrates

The ablated Ag substrates were characterized by specular reflectivity measurements using UV-visible spectrometer in the spectral range of 200–1000 nm. Plain silver substrates were used as the reference reflectors. UV-Vis reflection spectra of SS-1, SS-2, SS-3, and SS-4 are shown in Figure 7. Observed peak near 315 nm corresponds to interband transitions of "d" state electrons to the higher "s" or "p" states in Ag. Furthermore, a small peak was observed in the neighborhood of 340 nm for SS-1, SS-2. The spectral feature near 340 nm clearly indicates the formation of surface nanostructures with lateral dimensions comparable[73] to that of Ag NPs. Lau *et al.*[64,73] explained the presence of a broad peak (centered at 370 nm) in the absorption spectra of ps structured Ag target. The peak centered at 370 nm was an indication of Ag nanostructures on the laser exposed portion, which was confirmed through AFM observations of their structured surface. Further, oxidation of the nanostructured surface resulted in a red shift with a new peak at 400 nm. Analogous to this SS-1 and SS-2 exhibited a peak centered at 340 nm (and broadened towards the visible region) indicating the presence of lateral dimensional Ag NSs comparable to that of Ag NPs. This was confirmed from the FESEM images of laser irradiated SS-1 and SS-2 (see Figure 8). Moreover, position of the SPR peak depends on dielectric function of the material under consideration (Ag) and the surrounding medium (see equation below). The surrounding medium was air in the case of NSs and water in the case of NPs. Because of this, we could observe SPR peak near 340 nm for Ag nanostructures and near 400 nm for Ag colloidal solution.

$$\sigma_{ext} = \frac{9V\varepsilon_m^{\frac{3}{2}}}{c} \frac{\omega.\varepsilon_2(\omega)}{[\varepsilon_1(\omega) + 2.\varepsilon_m]^2 + \varepsilon_2(\omega)^2},$$

where V is the volume of the nanoparticle; ω is the frequency of light used, ε_1, ε_2 are real and imaginary parts of dielectric constant of the metal, respectively, and ε_m is the real part of the dielectric constant of the surrounding liquid.

We observed that the laser ablated portions of Ag substrates turned to permanent golden yellow which could be resultant of the collective oscillations of conduction electrons. The surface morphologies of the laser exposed portions of Ag substrates, characterized by FESEM, are presented in Figures

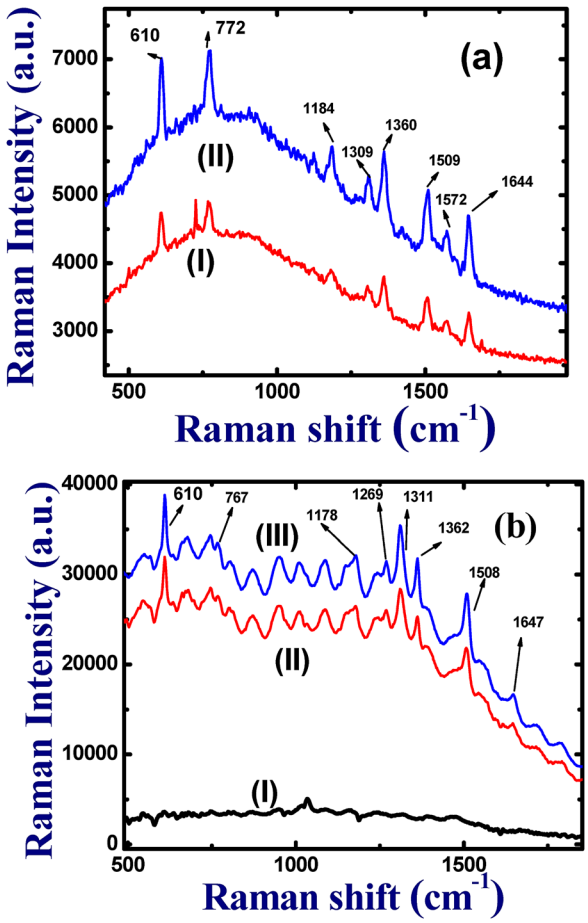

FIG. 10. Raman signals recorded from R6G molecules (12 μM) in methanol (a) with micro Raman spectrometer (excitation at 532 nm). Red, blue spectra represent the enhanced Raman signatures of R6G from SS-1 and SS-2, respectively (b) with bulk Raman spectrometer (excitation at 785 nm). Black spectrum was from Ag plain surface. Red, blue spectra represent the enhanced Raman signatures of R6G from SS-1 and SS-2. Signal collection time for both spectrometers was 5 seconds.

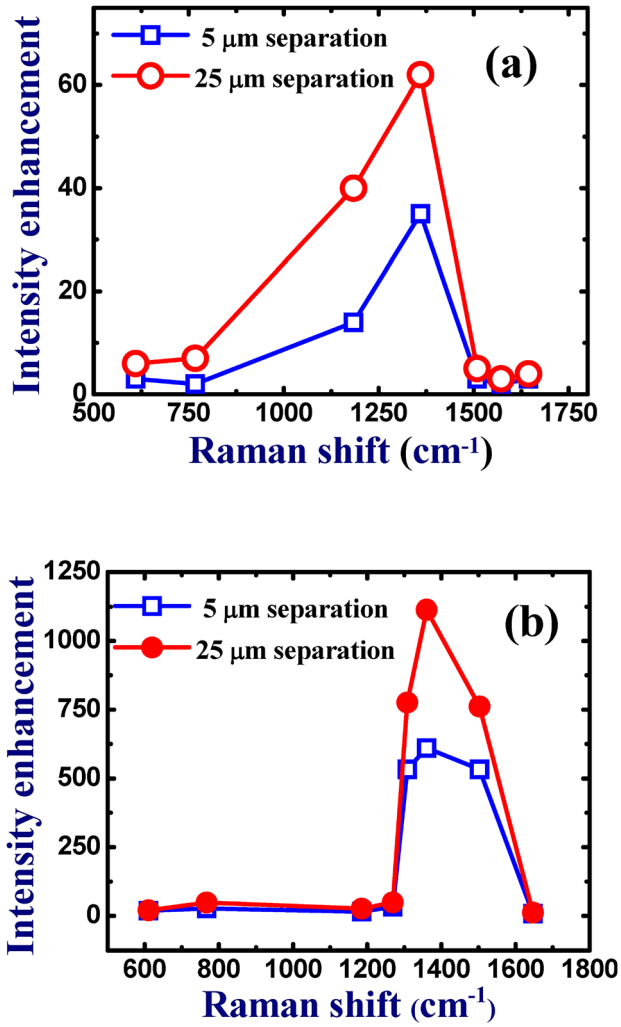

FIG. 11. Fluence versus Raman intensity enhancement observed from R6G adsorbed on the Ag substrates with excitation at (a) 532 nm (b) 785 nm. Symbols are experimental data points while lines are only a guide to the eye.

8(a)–8(d), depicting the nanostructures on SS-1 and SS-2 with dimensions of ~100 nm. There were no such nanostructures observed on SS-3 and SS-4 and was confirmed from FESEM images, depicted in Figure 9. Because of multiple/double ablation, we did not observe distinguishable demarcation between two consecutive structures in SS-1 and SS-2, whereas for SS-3 and SS-4, we could observe separation between the structures. As discussed in earlier sections, morphologies of

TABLE I. Observed active Raman modes of Rhodamine 6G adsorbed on Ag substrates SS-1 and SS-2 and their corresponding intensity enhancement obtained using excitation at 532 nm and 785 nm. Signal was collected for 5 seconds.

		Raman intensity enhancement in SERS spectra (Rhodamine 6G adsorbed on SS-1 and SS-2)					
R6G reported Raman modes (cm^{-1})	Assignments of active Raman modes	Observed modes for 532 nm excitation	Separation 5 μm	Separation 25 μm	Observed modes for 785 nm excitation	Separation 5 μm	Separation 25 μm
610	C-C-C ring in-plane bend	610	3	6	610	19	20
767	C-H out-plane bend	772	2	7	767	27	48
1185	C-C stretch	1184	14	40	1178	15	26
1269	C-O-C stretch	-	-	-	1269	33	48
1308	Not assigned	1309	-	-	1311	533	776
1360	Aromatic C-C stretch	1360	35	62	1362	610	1113
1503	Aromatic C-C stretch	1509	3	5	1508	533	761
1570	Aromatic C-C stretch	1572	2	3	-	-	-
1647	Aromatic C-C stretch	1644	3	4	1647	8	12

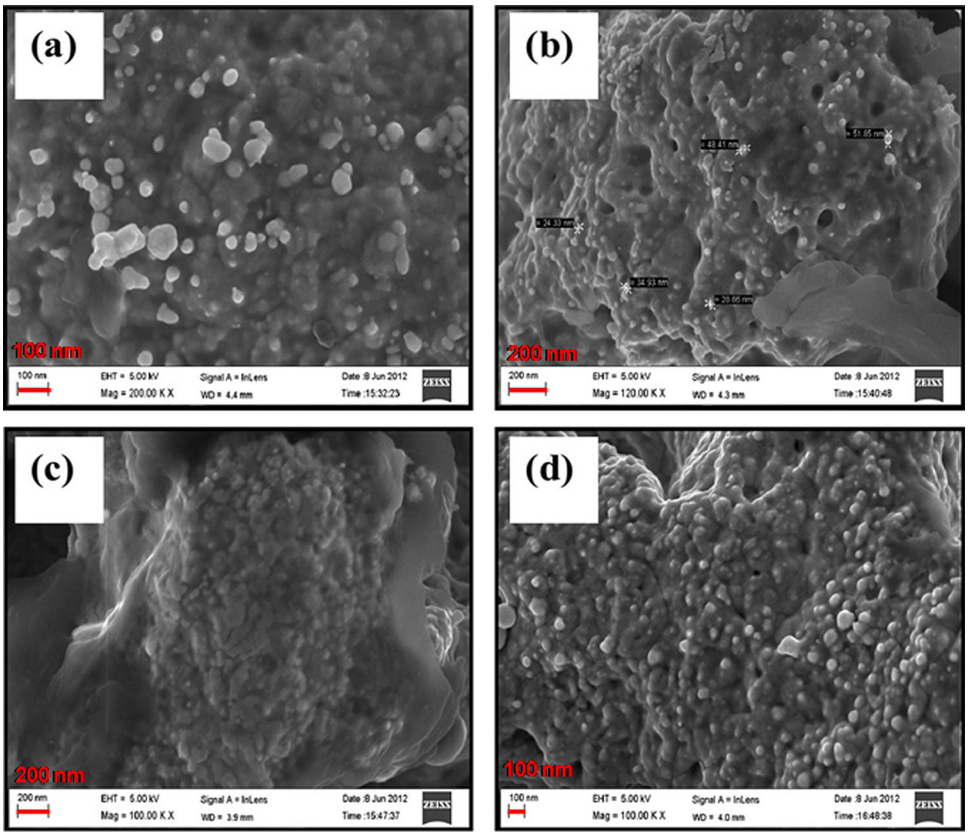

FIG. 12. FESEM images [closer view of the structure] of the laser exposed portions in Ag substrate in water prepared for diffrerent laser fluences (a) 4 J/cm^2, (b) 8 J/cm^2, (c) 12 J/cm^2, and (d) 16 J/cm^2. The images depict fabricated grains of Ag NPs on the substrate. The scale bar in (a) and (d) is 100 nm and for (b) and (c) it is 200 nm.

ablated metallic surfaces suffer from incubation effects.[74] The density and height of the nano-sized domes were different for SS-1 and SS-2. In addition to lateral nanostructures, there were small nanoparticle grains on both the substrates SS-1 and SS-2. These structures with Ag nanoparticle grains could enhance the Raman signals, and therefore, SS-1 and SS-2 were used for Raman measurements of adsorbed R6G molecules. These two substrates were used in Raman studies without further processing.

SERS is a surface spectroscopy indicating that adsorbed molecules only contributes to the Raman signal and enhancement of signal depends on the distance between the adsorbed molecule and tip of the nanostructure.[75,76] Nanostructures based SERS studies have been performed by Van Duyne *et al.* extensively.[77] It is rather difficult to compare the performance of different substrates prepared at different experimental conditions. Raman spectra recorded for R6G on the laser ablated surface SS-1 and SS-2 are shown in Figure 10(a) for 532 nm excitation and in Figure 10(b) for 785 nm excitation. Excitation with 785 nm demonstrated higher SERS enhancement (compared to 532 nm excitation) and lower fluorescence background from the analytes.[78–80] The dome-like nanostructures, probably, provided high local fields contributing to Raman signal enhancements. Raman signal intensity recorded for 1362 cm^{-1} mode of SS-1 excited with 785 nm was ~2439. However, the Raman signal intensity from the plain Ag surface was ~4. The intensity enhancement, therefore, was evaluated to be ~610. Raman signal enhancement for the 1362 cm^{-1} mode of SS-2 with 785 nm excitation was ~1113. For 532 nm excitation, intensity enhancements measured for the 1362 cm^{-1} were ~35 for SS-1 and ~62 for SS-2. Intensity enhancements of the other modes along with their mode assignments are shown in Table I. For R6G, the absorption peak is at 528 nm, which is in the vicinity of excitation wavelength 532 nm, pre-resonance effects resulted in strong fluorescence. The recorded Raman spectra of R6G from SS-3 and SS-4 with excitation wavelengths of 532 nm and 785 nm did not show any Raman signatures apart from fluorescence. From this observation, we concluded that the Ag substrates influenced by multiple/double ablation only provided Raman enhancement and single ablated surfaces could not. Raman signal enhancements plotted for SS-1 and SS-2 are shown in Figure 11. It was observed that superior signal enhancements were from SS-2 for both the excitation wavelengths 532 nm and 785 nm. Observations demonstrated that substrate with 25 μm line separations provided optimal Raman enhancements as a result of double ablation compared to substrate with 5 μm line separation on which multiple ablation took place. Probably, multiple ablation caused a partial washout of the substrate roughness compared to double ablation case. Measurements of R6G Raman enhancements revealed the performance of double ablated surface to be superior to multiply ablated surface. Therefore, we have concluded that scan separation of 25 μm provided optimal Raman enhancements as a result of double ablation. Based on this result, dependence of input laser fluence was studied in the double ablation case. For a fixed scan separation (25 μm), Ag substrates were ablated in distilled water for the fluences 4 J/cm^2, 8 J/cm^2, 12 J/cm^2, 16 J/cm^2, and 20 J/cm^2. Figures 12(a)–12(d) illustrate surface morphologies of Ag substrates fabricated at different fluences (for a fixed line separation 25 μm). Formation of Ag nanoparticle grains was again observed on these

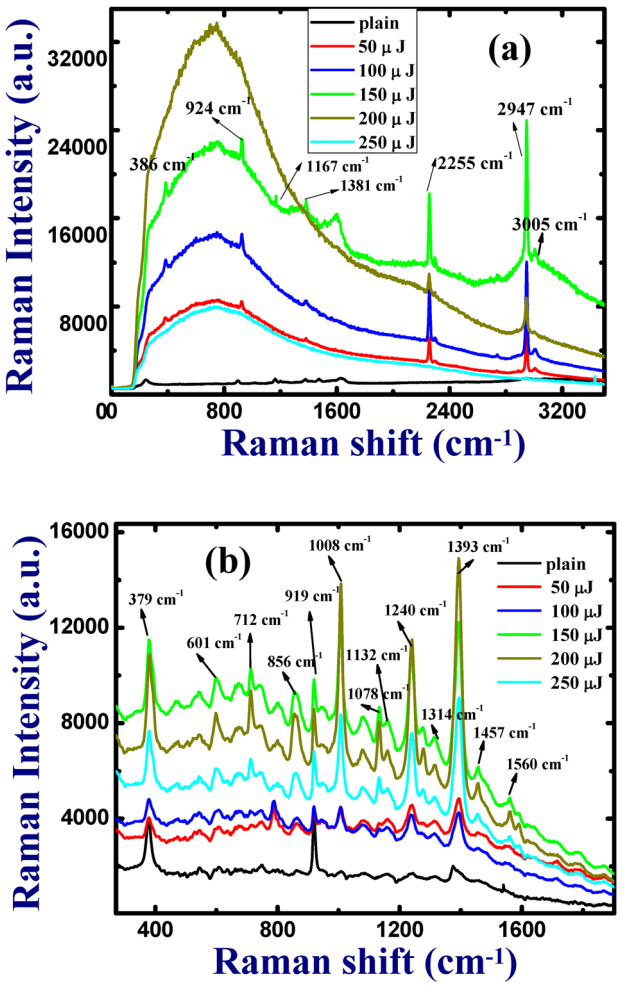

FIG. 13. (a) Micro-Raman spectra of adsorbed RDX molecules (excitation at 532 nm) in acetonitrile. The maximum enhancement of Raman signal was observed at pulse energy 150 μJ (fluence of 12 J/cm^2). (b) Bulk Raman spectra of the adsorbed RDX (excitation at 785 nm) in acetonitrile. The maximum enhancement of Raman signal was observed at pulse energy of 200 μJ (fluence of 16 J/cm^2). More signatures were observed with 785 nm excitation compared to 532 nm excitation. For both, the cases time of integration was 5 s.

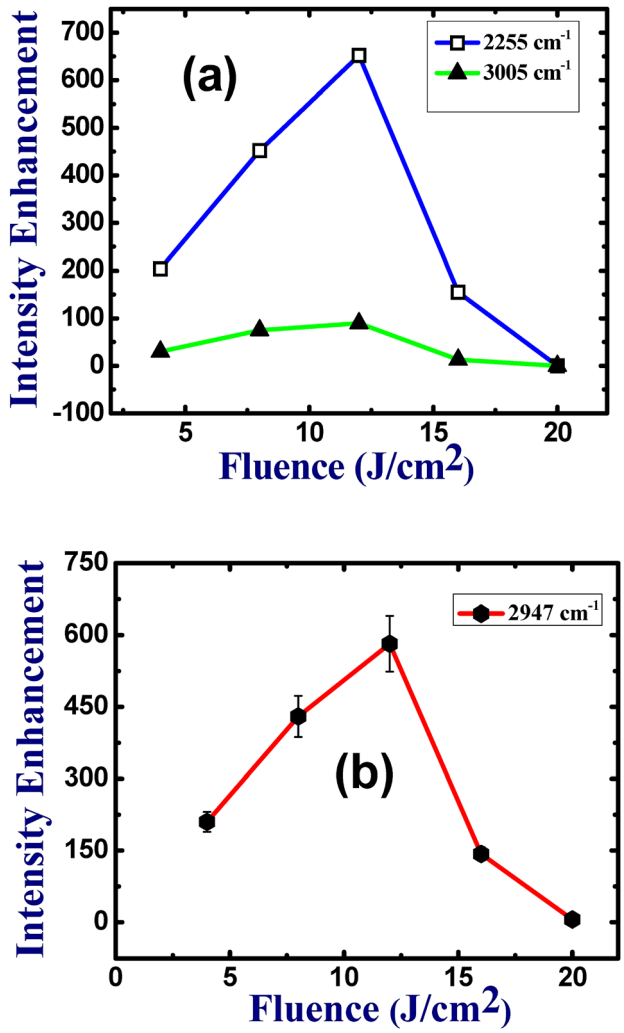

FIG. 14. Fluence versus Raman intensity enhancement observed from RDX adsorbed on the Ag substrates with excitation at 532 nm (a) 2255 cm^{-1} and 2005 cm^{-1} modes (b) 2947 cm^{-1} mode. Maximum enhancement was observed for the fluence 12 J/cm^2. Symbols are experimental data points while lines are only a guide to the eye.

substrates. SERS activity of these Ag substrates was investigated for RDX ($C_3H_6N_6O_6$; 1,3,5-Trinitroperhydro-1,3,5-triazine) molecules dissolved in acetonitrile. Raman spectra recorded for RDX analyte (dissolved in acetonitrile) adsorbed on the Ag substrates fabricated with different laser fluences are illustrated in Figures 13(a) and 13(b) for 532 nm and 785 nm excitations, respectively. The spectra were collected in the 250 cm^{-1} to 3500 cm^{-1} spectral range covering most of the Raman bands of RDX. Since the vibrational modes of analyte moieties adsorbed on the surface of Ag substrates are enhanced, typically fewer peaks[81–83] are observed in the SERS spectra compared to conventional Raman spectra. Raman signatures observed in the case of 785 nm excitation were higher compared to 532 nm excitation. 383 cm^{-1}, 924 cm^{-1} modes [Figure 13(a)] correspond to modes of acetonitrile and others are from RDX molecule. Raman intensity enhancements for different modes of RDX were measured as mentioned earlier. In the case 532 nm excitation, the modes corresponding to 2947 cm^{-1}, 2255 cm^{-1}, and 3005 cm^{-1} (C-H stretch) exhibit 582, 652, and 86 times of the enhancement, respectively. Some of the other modes observed were 1167 cm^{-1}, 1381 cm^{-1} (CH_2 twisting). However, fluorescence prevailed in the data obtained from substrates prepared at fluences of 16 J/cm^2 and 20 J/cm^2. In the case of 785 nm excitation [Figure 13(b)], some of the dominant modes were 856 cm^{-1} (N-N stretch + NO_2 axial scissoring), 924 cm^{-1} (CH_2 rocking or combination), 1240 cm^{-1} (N-N and symmetric NO_2 stretch and may be with CH_2 twist), 1314 cm^{-1} (N-N stretching CH_2 stretch), 1393 cm^{-1} (CH_2 twisting), 1457 cm^{-1} (CH_2 scissoring), 1560 cm^{-1} (ONO equatorial stretching). Assignments of the RDX modes were supported from the data obtained by Dregar *et al.*[84] Raman intensities for adsorbed RDX molecules were also evaluated as a function of input fluence. In the case of 532 nm excitation, strong Raman signal enhancement was observed from the Ag substrate fabricated at 12 J/cm^2 [Figures 14(a), 14(b)]. Figures 15(a)–15(c) illustrate Raman signal enhancement observed from the Ag substrates in the case of 785 nm excitation. All RDX modes were observed to have maximum enhancement from the Ag substrate fabricated at 16 J/cm^2. From the

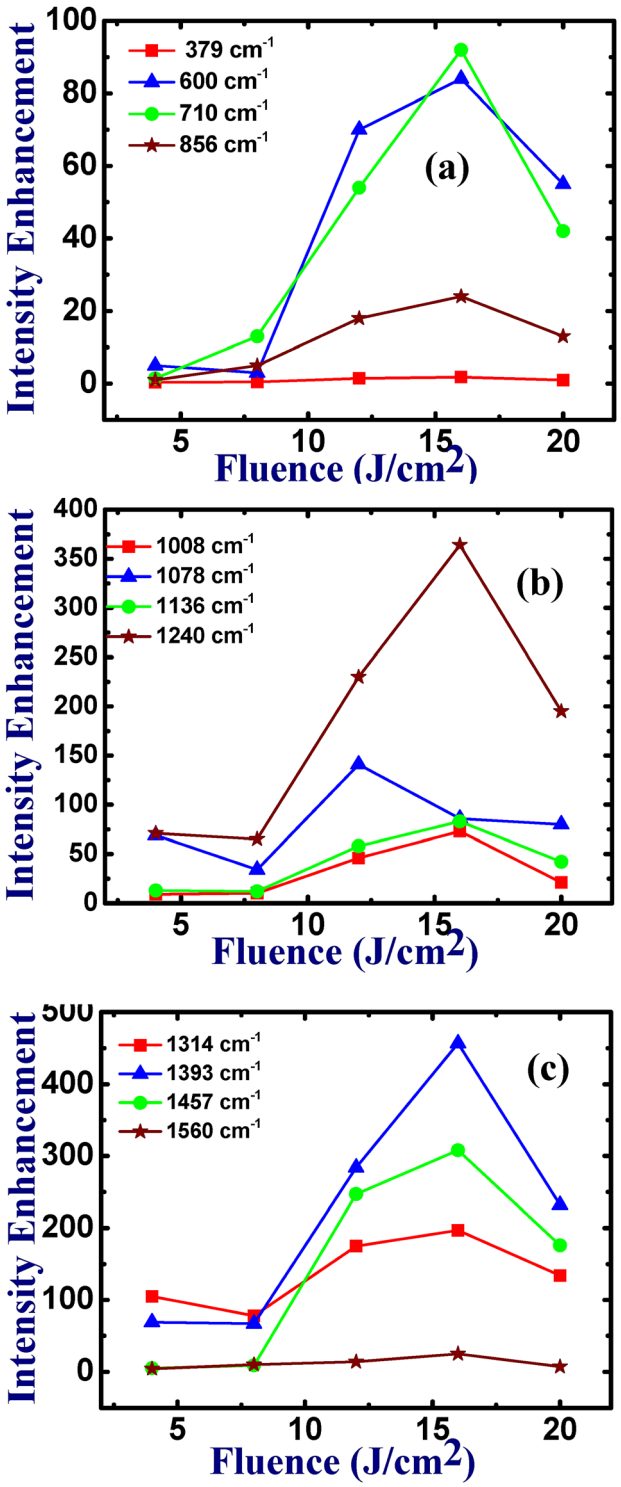

FIG. 15. Fluence versus Raman intensity enhancement for RDX Ag substrates with excitation at 785 nm for (a) 379 cm^{-1}, 600 cm^{-1}, 710 cm^{-1}, and 856 cm^{-1} modes (b) 1008 cm^{-1}, 1078 cm^{-1}, 1136 cm^{-1}, and 1240 cm^{-1} modes (c) 1314 cm^{-1}, 1393 cm^{-1}, 1457 cm^{-1}, and 1560 cm^{-1} modes. Maximum enhancement was observed for fluence of 16 J/cm^2 in most of the cases.

analysis of Raman signal enhancements of RDX with 532 nm, 785 nm excitation optimal fluences of 12 J/cm^2, 16 J/cm^2, respectively, were obtained. Intensity enhancement of the other modes of RDX is summarized in Table II. Oxidation layer and other contaminations from the substrates can be removed by cleaning with liquid ammonia and can use the substrates for number of times. Our future endeavor is to identify the optimum conditions for achieving efficient NPs and nanostructures for SERS applications by investigating the ablation procedure with (a) 60° incident laser beam (b) flow of liquid media while ablation.

TABLE II. Raman modes of RDX in ACN (~50 mM) adsorbed on different Ag substrates. Corresponding intensity enhancements are listed. Excitation wavelength was 785 nm. Signal was collected for 5 seconds.

Observed modes of RDX (in ACN) on Ag substrates	Raman signal intensity enhancement at different fluences				
	4 J/cm^2	8 J/cm^2	12 J/cm^2	16 J/cm^2	20 J/cm^2
601	5	3	70	84	55
712	1.5	13	54	92	42
856	1	5	18	25	13
1008	9	10	46	73	42
1078	69	34	141	86	80
1132	13	12	58	83	42
1240	71	65	250	364	195
1314	105	78	175	197	134
1393	69	67	284	457	232
1457	5	9	247	308	176
1560	2	3	10	25	7

CONCLUSIONS

Ultrafast laser ablation of metals submerged in liquid media offers size controllable, well dispersed nanoparticles along with nanostructured substrates in a single experiment. We succeeded in fabricating well dispersed Ag NPs and NSs using this technique. The nanostructures were observed predominantly in the regions where overwriting occurred. Double ablation is expected to play a crucial role in determining the hydrodynamic instabilities at the interface of vapor-melt, consequently the production of nanoparticles and nanostructures. NLO characterization of Ag water colloids revealed that 2PA prevailed at higher energies and corresponding NLO coefficients were obtained. Switching from SA at lower intensities to RSA at higher intensities is explained through the transitions of conduction group electrons to higher excited states. SERS spectra of R6G from SS-1 and SS-2 divulged that double ablation endowed favorable Raman signal intensities (SS-2) compared to multiple ablation (SS-1) and single ablation (SS-3, SS-4). In addition, laser fluence (4 J/cm^2, 8 J/cm^2, 12 J/cm^2, 16 J/cm^2, 20 J/cm^2) dependence on the fabrication of SERS active substrates has been investigated for the case of double ablation. It was observed that the maximum enhancement of Raman signals were observed from the RDX molecules adsorbed on Ag substrates fabricated at the fluences of 12 J/cm^2 (532 nm excitation) and 16 J/cm^2 (785 nm excitation). Ag nanoparticle grains in the nanostructures could possibly have generated hot spots for the observed signal enhancements. Moreover, we used the fabricated Ag substrate without any further treatment and this substrate preparation (typically 1 cm × 1 cm) can usually be performed in 30 minutes.

ACKNOWLEDGMENTS

We acknowledge the financial support of DRDO. We also acknowledge Mr. Ahmed, Centre for Nanotechnology, and Mr. Saikiran, and Mr. Lakshmi Narayana, School of Physics, for their assistance during characterization of some of these samples.

[1]S. L. Stoll, E. G. Gillan, and A. R. Barron, Chem. Vap. Deposition **2**, 182 (1996).
[2]S. Benerjee, S. Roy, J. W. Chen, and D. Chakravorthy, J. Magn. Magn. Mater. **219**, 45 (2000).
[3]R. W. Abdul and M. S. Seehra, Phys. Status Solidi A **193**, 94 (2002).
[4]K. Sturm, S. Fahler, and H. U. Krebs, Appl. Surf. Sci. **154**, 462 (2000).
[5]A. V. Simakin, V. V. Voronov, N. A. Kirichenko, and G. A. Shafeev, Appl. Phys. A **79**, 1127 (2004).
[6]E. Messina, E. Cavallaro, A. Cacciola, R. Saija, F. Borghese, P. Denti, B. Fazio, C. D'Andrea, P. G. Gucciardi, M. A. Lati, M. Meneghetti, G. Compagnini, V. Amendola, and M. Marago, J. Phys. Chem. C. **115**, 5115 (2011).
[7]V. Amendola, S. Polizzi, and S. Meneghetti, Langmuir **23**, 6766 (2007).
[8]M. Potara, M. Baia, C. Farcau, and S. Astilean, Nanotechnology **23**, 055501 (2012).
[9]I. Sur, M. Altunbek, M. Kahraman, and M. Culha, Nanotechnology **23**, 357102 (2012).
[10]U. K. Parashar, V. Kumar, T. Bera, P. S. Saxena, G. Nath, S. K. Srivastava, R. Giri, and A. Srivastava, Nanotechnology **22**, 415104 (2012).
[11]G. Krishna Podagatlapalli, S. Hamad, S. Sreedhar, S. P. Tewari, and S. Venugopal Rao, Chem. Phys. Lett. **530**, 93 (2012).
[12]P. V. Kazakevich, A. V. Simakin, and G. A. Shafeev, Quantum. Electron. **35**, 831 (2005).
[13]E. Stratakis, V. Zorba, M. Barberoglou, C. Fotakis, and G. A. Shafeev, Appl. Surf. Sci. **255**, 5346 (2009).
[14]E. Stratakis, M. Barberoglou, C. Fotakis, G. Viau, C. Garcia, and G. A. Shafeev, Opt. Express **17**, 12650 (2009).
[15]E. Stratakis, V. Zorba, M. Barberoglou, C. Fotakis, and G. A. Shafeev, Nanotechnology **20**, 105303 (2009).
[16]B. Kumar and R. K. Thareja, J. Appl. Phys. **108**, 064906 (2010).
[17]W. Philip, B. Stephan, B. Niko, and G. Particular, Laser Technol. Photonik Int. 20–22 (2011).
[18]M. D. Perry, B. C. Stuart, P. S. Banks, M. D. Feit, V. Yanovsky, and A. M. Rubenchik, J. Appl. Phys. **85**, 6803 (1999).
[19]D. Riabininan, M. Chaker, and J. Margot, Nanotechnology **23**, 135603 (2012).
[20]H. Zeng, X. W. Du, S. C. Singh, S. A. Kulinich, S. Yang, J. He, and W. Cai, Adv. Func. Mater **22**, 1333 (2012).
[21]Z. Yan and D. B. Chrisey, J. Photochem. Photobiol. C **13**, 204 (2012).
[22]L. D. Landau and E. M. Lifshitz, *Course of Theoretical Physics*, Vol. 6: Fluid Mechanics (Nauka, Moscow, 1986; Pergamon, New York, 1989).
[23]B. Kumar, D. Yadav, and R. K. Thareja, J. Appl. Phys. **110**, 074903 (2011).
[24]S. Barcikowski, A. Menendez-Manjon, B. N. Chichkov, M. Brikas, and G. Raclukaitis, Appl. Phys. Lett. **91**, 083113 (2007).
[25]N. Barsch, J. Jakobi, S. Weiler, and S. Barcikowski, Nanotechnology **20**, 445603 (2009).
[26]A. Menendez-Manjon, B. N. Chichkov, and S. Barcikowski, J. Phys. Chem. C. **114**, 2499 (2010).
[27]C. L. Sajti, R. Sattari, B. N. Chichkov, and S. Barcikowski, J. Phys. Chem. C. **114**, 2421 (2010).
[28]A. Crookell, M. Fleischmann, M. Hanniet, and P. J. Hendra, Chem. Phys. Lett. **149**, 123 (1988).
[29]D. B. Chase and B. A. Parkinson, Appl. Spectrosc. **42**, 1186 (1988).
[30]S. M. Angel, L. F. Katz, D. D. Archibald, and D. E. Hongis, Appl. Spectrosc. **43**, 367 (1989).
[31]M. Fleischman, P. J. Hendra, and A. McQuillan, J. Chem. Phys. Lett. **26**, 163 (1974).
[32]J. C. Tsang, J. R. Kirtely and J. A. Bradley, Phys. Rev. Lett. **43**, 772 (1979).
[33]M. Muniz-Miranda, C. Gellini, and E. Giorgetti, J. Phys. Chem. C **115**, 5021 (2011).
[34]J. G. Bergman, J. P. Heritage, A. Pinczuck, J. M. Worlock, and J. H. Mcfree, Chem. Phys. Lett. **68**, 412 (1979).
[35]J. E. Rowe, C. V. Shank, D. A. Zwemer, and C. A. Murray, Phys. Rev. Lett. **44**, 1770 (1980).
[36]T. H. Wood and M. V. Klein, Solid State. Commun. **35**, 263 (1980).
[37]J. G. Bergman, D. S. Chemla, P. F. Liao, A. M. Glass, A. Pinczuck, R. M. Hart, and D. H. Oslon, Opt. Lett. **6**, 33 (1981).
[38]E. Hutter and J. H. Fendler, Adv. Mater. **16**, 1685 (2004).
[39]M. Moscovits, J. Chem. Phys. **69**, 4159 (1978).
[40]E. Burstein, Y. J. Chen, C. Y. Chen, S. Lundquist, and E. Tosatti, Solid State Commun. **29**, 567 (1979).
[41]S. L. McCall, P. M. Platzman, and P. A. Wolf, Phys. Lett. A **77**, 381 (1980).
[42]J. I. Gersten and A. Nitzan, J. Chem. Phys. **73**, 3023 (1980).
[43]M. Kerker D. S. Wang, and H. Chew, Appl. Opt. **19**, 4159 (1980).
[44]C. K. Chen, R. B. de Castro A, and Y. R. Shen, Phys. Rev. Lett. **46**, 145 (1981).
[45]C. Gellini, M. Muniz-Miranda, M. Innocenti, F. Carlá, F. Loglio, M. L. Foresti, and P. R. Salvi, Phys. Chem. Chem. Phys. **10**(31), 4555 (2008).
[46]Z. Xu, J. Hao, W. Braida, D. Strickland, F. Li, and X. Meng, Langmuir **27**, 13773 (2011).
[47]H. Zhou, Z. Zhang, C. Jiang, G. Guan, K. Zhang, Q. Mei, R. Liu, and S. Wang, Anal. Chem. **83**, 6913 (2011).
[48]F. T. Docherty, P. B. Monaghan, C. J. McHugh, D. Graham, W. E. Smith, and J. M. Cooper, IEEE Sens. J. **5**, 632 (2005).
[49]S. Botti, L. Cantarini, and A. Paluccci, J. Raman Spectrosc. **41**, 866 (2010).
[50]I. Lee, S. W. Han, and K. Kim, J. Raman Spectrosc. **32**, 947 (2001).
[51]A. M. Manjon, P. Wagener, and S. Barcikowski, J. Phys. Chem. C **115**, 5108 (2011)
[52]M. Yin, H. P. Li, S. H. Tang, and W. Ji, Appl. Phys. B **70**(4), 587 (2000).
[53]S. Venugopal Rao, T. S. Prashant, T. Sarma, K. P. Pradeepta, D. Swain, and S. P. Tewari, Chem. Phys. Lett. **514**, 98 (2011).
[54]T. Sarma, P. K. Panda, P. T. Anusha, and S. Venugopal Rao, Org. Lett. **13**(2), 188 (2011).
[55]D. Swain, P. T. Anusha, T. S. Prashant, S. P. Tewari, T. Sarma, P. K. Panda, and S. Venugopal Rao, Appl. Phys. Lett. **100**, 141109 (2012).
[56]K. V. Saravanan, K. C. J. Raju, M. G. Krishna, S. P. Tewari, and S. Venugopal Rao, Appl. Phys. Lett. **96**, 232905 (2010).
[57]P. T. Anusha, S. Debasis, S. Hamad, T. S. Prashant, L. Giribabu, S. P. Tewari, and S. Venugopal Rao, J. Phys. Chem. C **116**, 17828 (2012).
[58]S. Hamad, S. P. Tewari, L. Giribabu, and S. Venugopal Rao, J. Porphyr. Phthalocyanines **16**, 140 (2012).
[59]F. Liang, R. Vallee, D. Gingras, and S. L. Chin, Opt. Mat. Exp. **1**, 1244 (2011).
[60]J. B. Nielsen, J. M. Savolainen, M. S. Christensen, and P. Balling, Appl. Phys. A **101**, 97 (2010).
[61]P. T. Mannion, J. Magee, E.Coyne, G. M. O'Conner, and T. J. Glynn, Appl. Surf. Sci. **233**, 275 (2004).
[62]J. K. Chen and J. E. Beraun, Numer. Heat Transfer, Part A **40**, 1 (2001).
[63]K. Furusawa, K. Taahashi, H. Kumagai, K. Midorikawa, and M. Obara, Appl. Phys. A **69**, S359 (1999).
[64]S. L. Truong, G. Levi, F. Bozon-Verduraz, A. V. Petrovskaya, A. V. Simakin, and G. A. Shafeev, App. Surf. Sci. **254**, 1236 (2007).
[65]E. Stratakis, Sci. Adv. Mater. **4**, 407 (2012).
[66]M. A. Garcia, J. Phys. D: Appl. Phys. **44**, 283001 (2011).
[67]D. C. Schinca, L. B. Scaffardi, F. A. Videla, G. A. Torchia, P. Moreno, and L. Roso, J. Phys. D: Appl. Phys. **42**, 215102 (2009).
[68]A. Moores and F. Goettmann, New. J. Chem. **30**, 1121 (2006).
[69]R. A. Ganeev, M. Baba, A. I. Ryasnyanskii, M. Suzuki, and H. Kuroda, Opt. Spectrosc. **99**, 668 (2005).
[70]M. Sheik-Bahae, A. A. Said, T. H. Wei, and D. J. Hagan, IEEE J. Quantum Electron. **26**, 760 (1990).
[71]R. L. Sutherland, *Handbook of Nonlinear Optics*, 2nd ed. (Marcel Dekker, New York, 2003).
[72]U. Gurudas, E. Brooks, D. M. Bubb, S. Heroith, T. Lippert, and A. Wokaun, J. Appl. Phys. **104**, 073107 (2008).
[73]S. L. Truong, G. Levi, F. Bozon-Verduraz, A. V. Petrovskaya, A. V. Simakin, and G. A. Shafeev, App. Phys A. **89**, 373 (2007).
[74]X. Ni, X. Ni, C. Wang, L. Yang, J. Li, L. Chai, W. Jia, R. Zhang, and Z. Zhang, Appl. Surf. Sci. **253**, 1616 (2006).
[75]R. Aroca, *Surface Enhanced Vibrational Spectroscopy* (John Wiley & Sons Ltd., Chichester, UK, 2006).
[76]S. Lal, N. K. Grady, G. P. Goodrich, and N. Halas, Nano. Lett. **6**, 2338 (2006).
[77]C. L. Haynes, A. D. McFarland, and R. P. Van Duyne, Anal. Chem. **77**, 338A (2005).
[78]C. M. Ruan, W. Wang, and B. H. Gu, J. Raman Spectrosc. **38**, 568 (2007).

[79]Y. Sawai, B. Takimoto, H. Nabika, and K. Ajito, Murakoshi Faraday Discuss. **132**, 179 (2006).
[80]K. Kneipp, H. Kneipp, and F. Sefert, Chem. Phys. Lett. **233**, 519 (1995).
[81]N. A. Hatab, G. Eres, P. G. Hatzinger, and B. Gu, J. Raman. Spectrosc. **41**, 1131 (2010).
[82]F. A. Calzzani, R. Sileshi, A. Kassu, J. M. Taguenang, A. Chowdhury, A. Sharma, P. B. Ruffin, C. Brantley, and E. Edwards, Proc. SPIE **6945**, 69451O (2008).
[83]R. J. Karpowicz and T. B. Brill, J. Phys. Chem. **88**, 348 (1984).
[84]Z. A. Dreger and Y. M. Gupta, J. Phys. Chem. B **111**, 3893 (2007).